Supplementary Information Titles

Please list each supplementary item and its title or caption, in the order shown below.

Note that we do NOT copy edit or otherwise change supplementary information, and minor (nonfactual) errors in these documents cannot be corrected after publication.
Please submit document(s) exactly as you want them to appear, with all text, images, legends and references in the desired order, and check carefully for errors.

Journal: Nature Medicine

Article Title:	**A Novel Technique for *In Vivo* Mapping of Myocardial Creatine Kinase Metabolism**
Corresponding Author:	Ravinder Reddy
Contributing Authors:	Mohammad Haris, Anup Singh, Kejia Cai, Feliks Kogan, Jeremy McGarvey, Catherine DeBrosse, Gerald A Zsido, Walter RT Witschey, Kevin Koomalsingh, James J Pilla, Julio A. Chirinos, Victor A. Ferrari, Joseph H Gorman, Hari Hariharan, Robert C Gorman, Ravinder Reddy

Supplementary Item & Number	**Title or Caption**
Supplementary Discussion	[NO DESCRIPTIVE TITLE NECESSARY
Supplementary Methods	[NO DESCRIPTIVE TITLE NECESSARY]

Supplementary Discussion

The chemical-exchange-saturation-transfer (CEST) technique has been widely used to map different metabolites and macromolecules *in vivo*[1-6]. Briefly, chemical exchange between bulk water and amine/amide/hydroxyl protons from different amino acids, proteins and other molecules have been exploited to measure pH *in vivo*[1], hepatic glycogen[2], cartilage glycosaminglycans[3], gene expression *in vivo*[4], myoinositol and glutamate in the brain [5,6].

Comparison with hyperpolarized ^{13}C MRI

Hyperpolarized ^{13}C MRI, using the techniques of parahydrogen induced polarization (PHIP) or dynamic nuclear polarization (DNP), has been used to study cardiac angiography, perfusion, catheter tracking and metabolic imaging[7,8]. It is worth comparing the CrEST technique with hyperpolarization as an alternative method for metabolic imaging. While the hyperpolarized ^{13}C MRI probes the pyruvate metabolic products such as lactate, alanine, bicarbonate, and carbon dioxide[8-10], it does not detect either free creatine (Cr), phosphocreatine (PCr) or their inter-conversion. The major advantages of hyperpolarized ^{13}C MRI is that due to its high signal to noise ratio (SNR) and zero background signal, it provides high contrast-to-noise-ratio images of a specific metabolite. However, due to the four times lower gyromagnetic ratio of ^{13}C compared to ^{1}H, it requires 4 times higher gradient strength that limits its resolution in its applications in large animals and humans. On the other hand, CrEST images water signal and can be performed on standard clinical scanners

(3T) without requirement of any additional gradient strength. Furthermore, ^{13}C NMR requires exogenous injection of the ^{13}C labeled pyruvate and other metabolites and on-site polarizing instrument while the CrEST exploits the endogenous Cr.

Tissue heterogeneity

In the current study, *ex vivo* tissues showed (30−40%) variation on CrEST contrast, which could be due to the intrinsic tissue heterogeneity as well as inhomogeneous tissue degradation caused by the delay between the animal sacrifice and experiment time. This variation can be minimized by reducing the 24 hours delay significantly.

Supplementary Methods

Animal handling and preparation

All animals were treated under experimental protocols approved by the University of Pennsylvania's Institutional Animal Care and Use Committee (IACUC) and in compliance with National Institutes of Health Publication No. 85−23, revised 1996.

Three male Yorkshire swine and two male Dorset sheep weighing between 35 and 40 kg were used in this study. For myocardial infarction (MI) creation (n = 3), animals were sedated with intramuscular ketamine injection (25−30 mg/kg), intubated, and mechanically ventilated. General anesthesia was maintained with

a mixture of inhaled isoflurane (1.5−3.0%) and oxygen, delivered by volume-controlled ventilation at a tidal volume of 10−15 ml/kg. Via a left thoracotomy, animals underwent selective ligation of the circumflex artery or its branches with non-absorbable suture to produce a postereolateral infarct of uniform shape involving approximately 20−25% of the left ventricular (LV) wall. Hemodynamic and echocardiographic data were recorded pre- and post-infarction. After ensuring hemodynamic and electrophysiologic stability, all animals were then recovered for anesthesia.

Prior to imaging, anesthesia was again initiated with ketamine and mixed isoflurane (1.5−3%) and maintained continuously throughout the imaging procedures. A high-fidelity pressure transducer (Millar Instruments, Houston, TX, USA) was guided into the left ventricle for cardiac gating. The animal was transported to a 3T MRI scanner connected to a ventilator and underwent cardiac imaging.

In vivo image acquisition protocol description

All animals were imaged at 3T Siemens scanner under an approved Institutional Animal Care and Use Committee (IACUC) protocol. The real challenge with *in vivo* cardiac experiments is tissue motion. This has been addressed in two ways: use of gated segmented image acquisition and use of z spectral fitting during post processing. Specialized hardware to provide combined respiratory and cardiac gating of image acquisition was used. Initial set up consisted of the following scans: (i) a general 3 plane multi-slice large FOV (50 cm) localizer, (ii) a smaller FOV (35−40 cm) oblique localizer to get the short axis heart orientation

and (iii) a multi-slice multi-phase Cine MRI scan with 12 phases along the short axis orientation. From the Cine images, the position and diastolic phase delay time for the slice of interest were determined. The diastolic phase delay time was used to fix the CEST acquisition protocol including trigger delay and the number of acquisition segments. The trigger delay time was adjusted such that the saturation duration and the acquisition duration fall in the diastolic phase. In the current study, after trigger delay, 250 ms saturation pulse was applied at peak B_{1rms} of 155 Hz (3.6 μT) followed by a ~50 ms readout period (8 segments with a segment TR ~6 ms) for a total time of ~300 ms. A delay of several seconds was allowed for the restoration of longitudinal magnetization, which was adjusted by respiratory gating.

We need images with about 48 saturation frequency offsets for z-spectral fitting. Each image acquisition with cardiac and respiratory gating takes about 16 respiratory periods (~ 48 s to 60 s based on the rate of respiration of animal) due to the need for keeping the segment size small enough (n = 8) to reduce motion artifacts. Thus the total acquisition time for the entire protocol is 40−48 minutes. The CrEST pulse sequence diagram is shown in Figure 1.

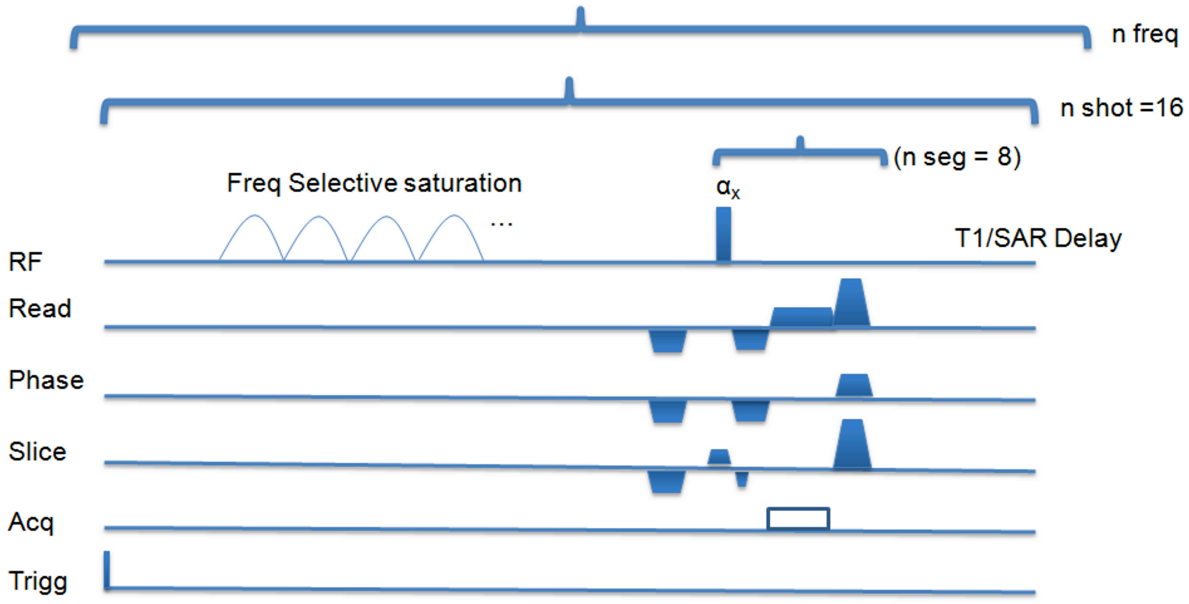

Figure 1. CrEST imaging pulse sequence.

The basic sequence consists of an outer shot loop containing the frequency selective saturation pulse train followed by an inner loop of segmented fast low angle shot (FLASH) gradient echo acquisitions and ending with a delay (T1/SAR delay). Shot loops are repeated using the number of shots required per image acquisition. In each shot 8 segments of k−space were acquired. The saturation pulse was applied just after trigger delay following the cardiac trigger pulse. We use a centric phase encoding order scheme to maintain the best CEST contrast. The whole sequence can be repeated to generate images with saturation applied at different offset frequencies.

In Vivo Myocardial Wall Identification

CEST weighted images obtained at +/-2 p.p.m. show good contrast between myocardial wall and chambers. Hence we used a manual procedure to identify the boundaries of myocardial wall as shown below in figure 2.

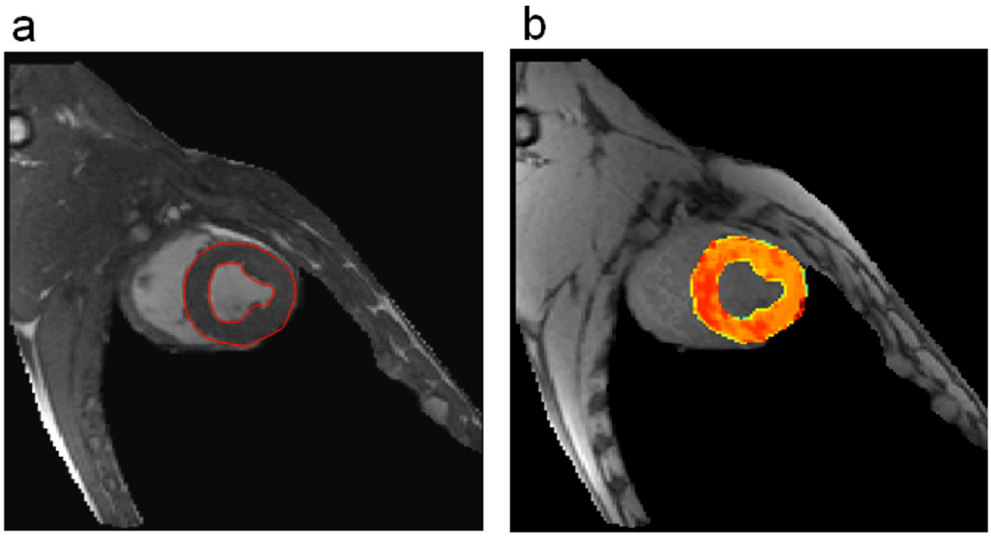

Figure 2. *In vivo* myocardial wall identification for color overlay. First, the myocardial wall was identified on anatomical CEST weighted image (2 p.p.m.) and was circumscribed manually (red polygon) as shown in (**a**) and a mask was generated. The CrEST map corresponding to the mask of myocardial wall was overlaid on the anatomical image without saturation as shown in (**b**).

Post Processing details

All image processing and data analysis was performed using in house written MATLAB (version 7.5, R2007b) routines. B_0 and B_1 maps were also obtained for the same slice position in case of *ex vivo* tissue and skeletal muscles and were used to correct the CEST asymmetry maps using the method described previously [5,6]. CrEST was computed using asymmetry analysis and normalized with negative frequency offset.

Background noise of image without saturation was removed by applying a threshold on signal intensity and a mask was generated. The mask was then applied on entire data to remove noise regions. Noise in image regions was reduced by applying an averaging kernel of size 3 × 3 spatially. After spatial noise reduction, data corresponding to both +ve and –ve frequencies over a limited range around ±1.8 p.p.m. were fitted, separately, with a linear function. The linear function was used to generate B_0 inhomogeneity corrected CEST images. Finally, the corrected CEST images were used to generate CrEST contrast map using asymmetry analysis as given in equation [1][6].

$$CrEST(\%) = 100 \times \left(\frac{S_{-ve} - S_{+ve}}{S_{-ve}} \right) \qquad \text{Eq [1]}$$

where S_{-ve} and S_{+ve} are the B_0 inhomogeneity corrected MR signals at -1.8 p.p.m. and +1.8 p.p.m. respectively. To account for and minimize the contribution from direct saturation and magnetization transfer effects, we used S_{-ve} instead of S_0 for normalization.

The animal data with more than 10% heart rate fluctuation and/ or more than 2 mm heart wall displacement during the course of imaging were excluded from this study. Even on the included data, CEST contrast obtained by asymmetry analysis is somewhat unreliable due to subtraction artifacts caused by residual respiratory and left ventricular wall motion and fluctuations of B_0 during gated CEST imaging. z-spectral fitting based methods can mitigate these artifacts. In this study, we adopted an approach of fitting a probabilistic combination of Lorentzian functions, corresponding to direct saturation (DS), magnetization

transfer (MT) and CrEST components as described below. This model is a modification to the previously published combination of Lorentzian functions for CEST z-spectral fitting[11].

Probabilistic model (PM) for z-spectrum

Let A, B and C are non-mutually exclusive events. According to additive law of probability[12], the probability of union of these three events is given by following equation:

$$p(A \cup B \cup C) = p(A) + p(B) + p(C) - [p(A \cap B) + p(B \cap C) + p(A \cap C)] + p(A \cap B \cap C) \quad \text{Eq [2]}$$

where 'U' and '∩' represents union and intersection respectively.

Since DS, MT and CrEST are non- mutually exclusive events, probability of union of these events can be obtained using equation [2]. Z-spectrum corresponds to the probability distribution of union of DS, MT and CrEST. Let's assume Lorentzian (L_i, i = 1,2, 3) distributions for DS, MT and CrEST.

$$L_i(x, A_i, W_i, C_i) = A_i \times \frac{\left(\frac{W_i^2}{4.0}\right)}{\left(\frac{W_i^2}{4.0}\right) + (x - C_i)^2} \quad \text{Eq [3]}$$

Where, A =amplitude, W=width, C =center of Lorentzian, x =offset frequency.

Using probabilistic model and Lorentzian functions corresponding to DS, MT and CrEST events, the following equations are used to fit z-spectral data over [-5, 5] p.p.m. frequency offset range:

$$f = 1 - p(DS \cup MT \cup CrEST) \quad \text{Eq [4]}$$

$$f(x) = 1 - \left\{ \sum_{i=1}^{3} L_i(x) - \sum_{i=1, j>i}^{3} \left(L_i(x) \times L_j(x) \right) + \prod_{i=1}^{3} L_i(x) \right\} \qquad \text{Eq [5]}$$

Where x is frequency offset? The center of CEST component was fixed at 1.8 p.p.m. relative to DS center.

The PM model fitting was validated for z-spectral data obtained using standard 3-pool model Bloch equations with exchange terms[13]. Next, we experimentally demonstrated the equivalent performance of this approach to the standard asymmetry analysis using *ex vivo* tissue results. *Ex vivo* Z-spectral data over -5 to 5 p.p.m. range were fitted with PM function using a non-linear fitting routine in MATLAB (lsqnonlin) as shown in Figure 3 below.

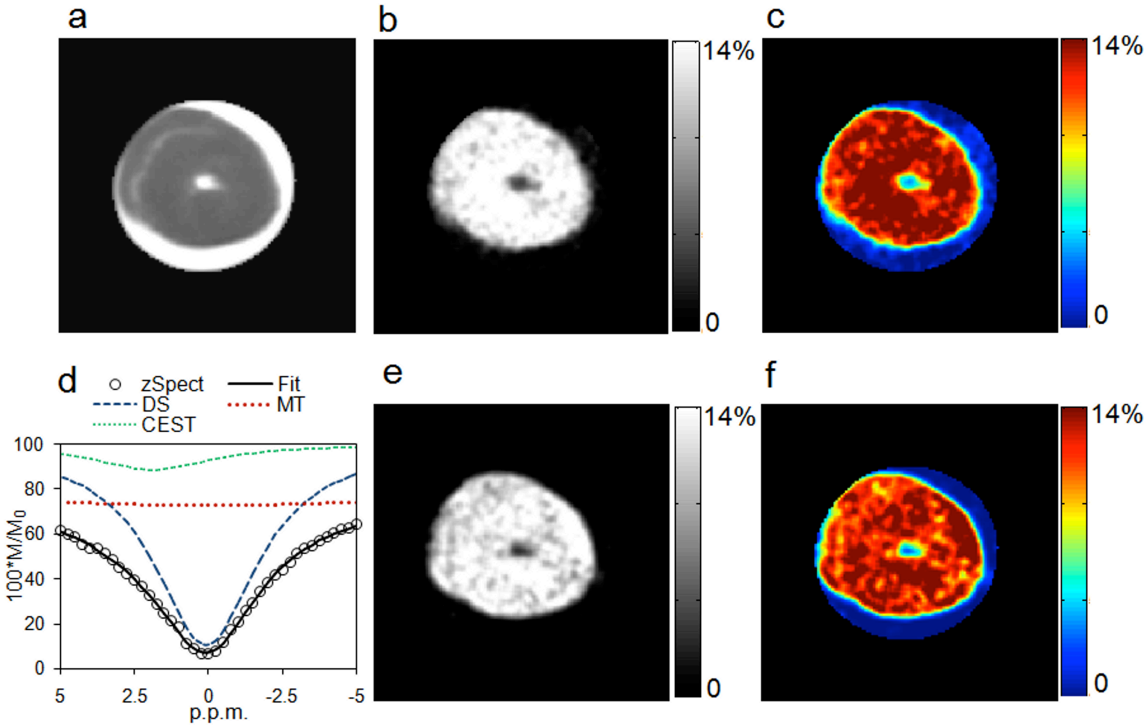

Figure 3. *Ex vivo* tissue data: Anatomical CEST weighted image (2 p.p.m.) of a non-infarcted lamb myocardium (**a**). gray scale and color coded CrEST contrast map generated through asymmetry-based analysis (**b, c**). Fitting of z-spectra

along with fitted components (DS, direct water saturation; MT, magnetization transfer; and CEST) in a voxel in *ex vivo* tissue using PM model. Gray scale and color coded CrEST map of the same tissue obtained using PM based approach (**e, f**). The CrEST contrast calculated using both approaches are comparable and within ~10% of variation.

Procedure for PM fitting in vivo data:

Here we adopted a two-step fitting procedure. In the first step, z-spectra corresponding to 4 small ROIs on the myocardial wall are fitted and the results from the ROI with the best fit are used to set constraints and initial guess for voxel wise z-spectra fitting of entire myocardium tissue. Upper and lower bound for constraints were set at ±10% of the initial guess. In cases of animals with infarct, ROIs were drawn in both healthy and infarcted regions and best-fit parameters were obtained separately for both types of tissues.

Scan time considerations

There is a substantial difference in total scan times between *in vivo* skeletal muscle and *in vivo* cardiac studies. In the case of cardiac studies, we need images with about 48 saturation frequency offsets for z-spectral fitting. Each image acquisition with cardiac and respiratory gating takes about 16 respiratory periods (~ 48 s to 60 s based on the rate of respiration of animal). Thus the total acquisition time for the entire protocol is 40−48 minutes. In the case of skeletal muscle, since the data are acquired in the absence of motion, we can use CEST

asymmetry analysis with B_0 correction as given in Equation 1. This requires a total of 6 saturation-offset frequencies (3 on the positive side and 3 on the negative side). We also use a single shot readout of a whole image with respect to saturation pulse with a TR of 4 s for each offset frequency. Hence, in the case of calf muscle, in essence, we can gather the CrEST map in about 24 s. The B_0 and B_1 maps collected either pre- or post exercise can be used for correcting the B_0 and B_1 field heterogeneities.

Spectroscopy data processing

^{1}H and ^{31}P MR spectra were phased and baseline corrected and fitted using nonlinear least-squares method with Gaussian functions. Unsuppressed water signal from the same voxel was used to derive absolute concentration of creatine in tissue as well as PCA extracts.

Sample size

As this is a methodology development study, the sample sizes were chosen to illustrate feasibility and no randomization or group categorization was done.

References:

1. Zhou, J., Payen, J.F., Wilson, D.A., Traystman, R.J. & van Zijl, P.C. Using the amide proton signals of intracellular proteins and peptides to detect pH effects in MRI. *Nat Med* **9**, 1085-1090 (2003).
2. van Zijl, P.C., Jones, C.K., Ren, J., Malloy, C.R. & Sherry, A.D. MRI detection of glycogen in vivo by using chemical exchange saturation transfer imaging (glycoCEST). *Proc Natl Acad Sci U S A* **104**, 4359-4364 (2007).
3. Ling, W., Regatte, R.R., Navon, G. & Jerschow, A. Assessment of glycosaminoglycan concentration in vivo by chemical exchange-dependent saturation transfer (gagCEST). *Proc Natl Acad Sci U S A* **105**, 2266-2270 (2008).
4. Gilad, A.A.*, et al.* Artificial reporter gene providing MRI contrast based on proton exchange. *Nat Biotechnol* **25**, 217-219 (2007).
5. Haris, M., Cai, K., Singh, A., Hariharan, H. & Reddy, R. In vivo mapping of brain myo-inositol. *NeuroImage* **54**, 2079-2085 (2011).
6. Cai, K.*, et al.* Magnetic resonance imaging of glutamate. *Nature medicine* **18**, 302-306 (2012).
7. Tyler, D.J. Cardiovascular Applications of Hyperpolarized MRI. *Current cardiovascular imaging reports* **4**, 108-115 (2011).
8. Golman, K.*, et al.* Cardiac metabolism measured noninvasively by hyperpolarized 13C MRI. *Magnetic resonance in medicine : official journal of the Society of Magnetic Resonance in Medicine / Society of Magnetic Resonance in Medicine* **59**, 1005-1013 (2008).
9. Merritt, M.E.*, et al.* Hyperpolarized 13C allows a direct measure of flux through a single enzyme-catalyzed step by NMR. *Proceedings of the National Academy of Sciences of the United States of America* **104**, 19773-19777 (2007).
10. Lau, A.Z.*, et al.* Rapid multislice imaging of hyperpolarized 13C pyruvate and bicarbonate in the heart. *Magnetic resonance in medicine : official journal of the Society of Magnetic Resonance in Medicine / Society of Magnetic Resonance in Medicine* **64**, 1323-1331 (2010).
11. Zaiss, M., Schmitt, B. & Bachert, P. Quantitative separation of CEST effect from magnetization transfer and spillover effects by Lorentzian-line-fit analysis of z-spectra. *J Magn Reson* **211**, 149-155 (2011).
12. Dennis D. Wackerly, William Mendenhall & Scheaffer, R.L. *Mathematical Statistics with Applications*.
13. Woessner, D.E., Zhang, S., Merritt, M.E. & Sherry, A.D. Numerical solution of the Bloch equations provides insights into the optimum design of PARACEST agents for MRI. *Magnetic resonance in medicine : official journal of the Society of Magnetic Resonance in Medicine / Society of Magnetic Resonance in Medicine* **53**, 790-799 (2005).